Topology optimization for elastic buckling of structures at macro- and micro-scales

Mariana Figueiredo
mariana.a.figueiredo@tecnico.ulisboa.pt

Instituto Superior Técnico, Universidade de Lisboa, Portugal

January 2021

Abstract

The stability problem of structures built from periodic cellular materials and the problem of obtaining optimal structures with maximized buckling strength are here addressed. The stability problem is considered at micro-, macro- and mixed-scales by means of a linearized buckling theory. When considering the macro-scale problem, the effective properties are obtained from the homogenization theory. To address the mixed-scale problem, the proposed methodology is obtained by applying the same finite element discretization to macro- and micro-scale domains. The solution for maximum buckling strength of structures is obtained by topology optimization with a density based approach, where no multiplicity of eigenvalues is included. The used design variables updating scheme is the Method of Moving Asymptotes. The computational implementations are applied to benchmark examples and the results are compared with similar ones found in the literature. The implementation of the coupled instability problem enables the application of the coupled instability equation. Similar results, as far as the author knows, do not exist in the literature.

Keywords: Multi-scale Buckling, Cellular Materials, Homogenization, Topology Optimization, Finite Elements

1. Introduction

Buckling occurs when a structure is subjected to a gradually increasing load that, after reaching some critical value, results in a sudden change of its equilibrium configuration. This static equilibrium position modification, causes the vanishing of the structure's stiffness and may occur before the structure starts to yield or fails. This means that when a component of an given assembly buckles, the remaining ones support the load beyond this critical value.

In the aerospace sector, since weight plays a crucial role, lightweight structures are widely used and their inherent slenderness makes stability one of the key requirements when designing aerospace structures.

Lightweight structures are typically built from low density cellular materials whose strength capacity is also limited by micro-structural instabilities, which may occur when their slender structural members are subjected to compressing loads [1]. Thus, structures built with these materials can buckle on multi spacial scale levels (macro-scale, micro-scale and mixed-scale levels).

There is, therefore, the need to design structures as well as materials for improved buckling performance. One of the most attractive ways of finding optimal designs is topology optimization, since it doesn't rely on any preconceived shape of the structure. In fact, topology optimization "has been recognized as one of the most effective approaches at the conceptual design phase of most engineering applications" [2].

In the context of buckling strength of periodic materials, Neves et al. [3] proposed a methodology for using topology optimization for the maximization of the critical load for micro-structures exhibiting micro-scale buckling modes with the same periodicity of the cellular material. Later, this work was extend to include buckling modes of different wavelengths by means of the complete Bloch-wave theory [1].

As for the macro-scale buckling strength of structures based on continuum models, optimality conditions for single and multiple eigenvalues are presented in [4] and a methodology for the maximization of the linearized buckling load using topology optimization is presented in [5]. A recent review on the topic of topology optimization addressing buckling can be found in [6].

It can then be understood that the application of topology optimization in the industrial environment

is still quite an open topic and that that is even more evident when addressing the stability of structures. Furthermore, while computational models as well as studies have been developed for the calculation and optimization of linearized buckling loads at macro- and micro-scale levels (even though not very extensively), no such implementations were found for the mixed-scale buckling case.

This work aims, then, to answer to the question of how to calculate and implement the buckling response of a structure built from solids with periodic materials based on a linearized stability theory. This includes a brief review of the existing methods for addressing buckling at separated macro- and micro-scales as well as the study and implementation of the mixed-scale problem. Furthermore, on the topic of obtaining optimal designs, this work focuses only on macro-scale structural optimization for the maximization of buckling strength.

In sections 2 and 3, the used linearized stability theory and optimization formulation are presented. Section 4 is focused on the description of the carried-out studies and numerical computations. The results from the application of the carried-out implementations are presented in section 5, together with some verification examples, whenever possible. In sections 6 and 7, the main conclusions of this work are summarized and some comments and reflections on futures works to be addressed are made.

2. Linear elastic buckling theory for solids with periodic micro-structure

The stability problem is here analyzed by means of a linearized theory based in [7] and [8] and the references therein.

Let a linear-elastic body be defined by a domain Ω^ε and a boundary Γ, being quasi-statically loaded with: prescribed displacements in Γ_u, surface tractions $\boldsymbol{t}$ in Γ_t and body forces $\boldsymbol{f}$ in Ω^ε. The superscript ε indicates a dependency on the micro-structure, as it is defined as the unit cell scale parameter, $\varepsilon = \frac{d}{D} \ll 1$, where d is a characteristic dimension of the unit cell and D a characteristic dimension of the structure.

The loading is gradually increased, only applied at the macro-scale level and also considered proportional to some reference loading, $\boldsymbol{t} = \lambda \boldsymbol{t^{ref}}$ and $\boldsymbol{f} = \lambda \boldsymbol{f^{ref}}$.

Assuming the body has a uniform micro-structural shape, the solid can be represented by a periodic repetition of a unit cell, defined by the domain $Y =]0, Y_1[\mathrm{x}]0, Y_2[\mathrm{x}]0, Y_3[$ and, here, built from a base material with holes in it. This base material is homogeneous, linear-elastic and isotropic, meaning that the constitutive relations can be given by the generalized Hooke's law, $\sigma_{ij}(\boldsymbol{u^\varepsilon}) = E_{ijkm} e_{km}(\boldsymbol{u^\varepsilon})$, where $\boldsymbol{\sigma}$ and $\boldsymbol{e}$ are the stress and strain tensors, respectively, and $\boldsymbol{E}$ is the constitutive matrix.

The equilibrium positions can be given by the minimization of the total potential energy, given by

$$\Pi(\boldsymbol{u}^\varepsilon) = A(\boldsymbol{u}^\varepsilon) - R(\boldsymbol{u}^\varepsilon), \tag{1}$$

where $A(\boldsymbol{u^\varepsilon})$ is the total elastic strain energy and $R(\boldsymbol{u^\varepsilon})$ is the applied forces potential defined as

$$A(\boldsymbol{u}^\varepsilon) = \frac{1}{2} \int_\Omega E_{ijkm} e_{km}(\boldsymbol{u}^\varepsilon) e_{ij}(\boldsymbol{u}^\varepsilon) d\Omega, \tag{2}$$

$$R(\boldsymbol{u^\varepsilon}) = \lambda \int_\Omega f_i^{ref} u_i^\varepsilon d\Omega + \lambda \int_{\Gamma_t} t_i^{ref} u_i^\varepsilon d\Gamma, \tag{3}$$

where

$$e_{ij}(\boldsymbol{u}^\varepsilon) = \frac{1}{2}\left(\frac{\partial u_i^\varepsilon}{\partial x_j} + \frac{\partial u_j^\varepsilon}{\partial x_i}\right) + \frac{1}{2}\left(\frac{\partial u_k^\varepsilon}{\partial x_i}\frac{\partial u_k^\varepsilon}{\partial x_j}\right). \tag{4}$$

The displacement field, which is a function of both the macro-spatial, $\boldsymbol{x}$, and micro-spatial, $\boldsymbol{y}$, variables, is represented using an infinitesimal real displacement parameter α:

$$\boldsymbol{u}^\varepsilon = \boldsymbol{u}^{0\varepsilon} + \alpha \boldsymbol{u}^{1\varepsilon}, \tag{5}$$

where $\boldsymbol{u^{0\varepsilon}}$ is the displacement related with the unique primary equilibrium configuration and $\boldsymbol{u^{1\varepsilon}}$ is a relative displacement, which, when multiplied by α, represents the possible "jump" to the secondary equilibrium position.

Based on the periodicity of the material, it is assumed that the displacement field terms can be expressed by asymptotic expansions in terms of the scale parameter ε,

$$\boldsymbol{u}^{0\varepsilon}(\boldsymbol{x},\boldsymbol{y}) = \boldsymbol{u}^{00}(\boldsymbol{x},\boldsymbol{y}) + \varepsilon \boldsymbol{u}^{01}(\boldsymbol{x},\boldsymbol{y}) + \varepsilon^2 \boldsymbol{u}^{02}(\boldsymbol{x},\boldsymbol{y}) + ..., \tag{6}$$

$$\boldsymbol{u}^{1\varepsilon}(\boldsymbol{x},\boldsymbol{y}) = \boldsymbol{u}^{10}(\boldsymbol{x},\boldsymbol{y}) + \varepsilon \boldsymbol{u}^{11}(\boldsymbol{x},\boldsymbol{y}) + \varepsilon^2 \boldsymbol{u}^{12}(\boldsymbol{x},\boldsymbol{y}) + ..., \tag{7}$$

$$\boldsymbol{y} = \frac{\boldsymbol{x}}{\varepsilon},$$

where the functions $\boldsymbol{u}^{ab}$ with indices a=0,1 and b=0,1,2,... are assumed Y-periodic (have the same periodicity as the unit cell).

The minimization of the total potential energy is expressed by

$$\delta\Pi(\boldsymbol{u}^\varepsilon) = \delta A(\boldsymbol{u}^\varepsilon) - \delta R(\boldsymbol{u}^\varepsilon) = 0. \tag{8}$$

Performing the differentiation of Y-periodic functions as in [8] $\frac{d}{dx_j}F(\boldsymbol{x},\boldsymbol{y}) = \frac{\partial F(\boldsymbol{x},\boldsymbol{y})}{\partial x_j} + \frac{1}{\varepsilon}\frac{\partial F(\boldsymbol{x},\boldsymbol{y})}{\partial y_j}$, considering only the first two terms of the asymptotic expansions (6) and (7) and introducing a perturbation $\delta u^\varepsilon = \alpha\{\boldsymbol{v}^{10}(\boldsymbol{x},\boldsymbol{y}) + \varepsilon \boldsymbol{v}^{11}(\boldsymbol{x},\boldsymbol{y}) + ...\}$, where $\boldsymbol{v}^{10}$ and $\boldsymbol{v}^{11} \in V_{\Omega\times Y} = \{\boldsymbol{v}(\boldsymbol{x},\boldsymbol{y}) : \boldsymbol{v}|_{\Gamma_u} = 0$ and $\boldsymbol{v}$ is Y-periodic$\}$, equation (8) becomes (separated in terms of α powers)

$$\alpha \int_{\Omega^\varepsilon} E_{ijkm}\{e_{ij}^0(\boldsymbol{u}^\varepsilon) e_{km}^I(\boldsymbol{v}^\varepsilon)\} d\Omega -$$

$$-\alpha\lambda\int_{\Gamma_t}\boldsymbol{t}_i\boldsymbol{v}_i^{\varepsilon}d\Gamma-\alpha\lambda\int_{\Omega^{\varepsilon}}\boldsymbol{f}_i\boldsymbol{v}_i^{\varepsilon}d\Omega=0\;\forall\;\boldsymbol{v}\in V_{\Omega\times Y},\tag{9}$$

$$\alpha^2\int_{\Omega^{\varepsilon}}E_{ijkm}\{e_{ij}^0(\boldsymbol{u}^{\varepsilon})e_{km}^{II}(\boldsymbol{v}^{\varepsilon})+e_{ij}^0(\boldsymbol{v}^{\varepsilon})e_{km}^{II}(\boldsymbol{u}^{\varepsilon})+$$

$$+e_{ck}^I(\boldsymbol{u}^{\varepsilon})e_{cm}^I(\boldsymbol{v}^{\varepsilon})+e_{ck}^I(\boldsymbol{v}^{\varepsilon})e_{cm}^I(\boldsymbol{u}^{\varepsilon})\}d\Omega=0\tag{10}$$

$$\forall\;\boldsymbol{v}\in V_{\Omega\times Y}.$$

where $e_{ij}^0(\boldsymbol{u}^{\varepsilon})$, $e_{ij}^I(\boldsymbol{u}^{\varepsilon})$ and $e_{ij}^{II}(\boldsymbol{u}^{\varepsilon})$ are the terms in α^0, α^1 and α^2 of the strain tensor (see [7]).

The equations that characterize the small elastic deformation before bifurcation are obtained from the analysis of equation (9). The analysis is performed by grouping the terms in ε powers and setting each of them to zero.

From the term in ε^{-2}, it can be shown that

$$\boldsymbol{u}^{00}(\boldsymbol{x},\boldsymbol{y})=\boldsymbol{u}^{00}(\boldsymbol{x}).\tag{11}$$

From the term in ε^{-1}, acknowledging that $\boldsymbol{v}$ are independent variations that can assume any value, ε is very small and $\boldsymbol{u}^{00}$, $\boldsymbol{u}^{01}$, $\boldsymbol{v}^{10}$ are periodic functions in $\boldsymbol{y}$ and using result (11), one obtains

$$\boldsymbol{u}_i^{01}(\boldsymbol{x},\boldsymbol{y})=-\chi_i^{km}(\boldsymbol{y})\frac{\partial u_k^{00}(\boldsymbol{x})}{\partial x_m}.\tag{12}$$

To satisfy the previous equation, the characteristic displacements χ_i^{km} must be the solution of the km static problems at micro-scale level,

$$\int_Y E_{ijpq}\frac{\partial\chi_i^{km}}{\partial y_q}\frac{\partial v_i}{\partial y_j}dY=\int_Y E_{ijkm}\frac{\partial v_i}{\partial y_j}dY,\tag{13}$$

$$\forall\;\boldsymbol{v}\in V_Y=\{\boldsymbol{v}\text{ is Y-periodic}\},$$

where periodic displacements at the unit cell's boundary are prescribed.

As for the term in ε^0, using previous results, the equation expressing macroscopic static equilibrium is obtained,

$$\int_{\Omega^{\varepsilon}}\frac{1}{|Y|}\int_Y\left(E_{ijkm}-E_{ijpq}\frac{\partial\chi_p^{km}}{\partial y_q}\right)dY\frac{\partial u_k^{00}}{\partial x_m}\frac{\partial v_i^{10}}{\partial x_j}d\Omega=$$

$$=\lambda\int_{\Gamma_t}t_i^{ref}v_i^{10}d\Gamma+\lambda\int_{\Omega^{\varepsilon}}f_i^{ref}v_i^{10}d\Omega,\;\forall\;\boldsymbol{v}^{10}\in V_{\Omega}.\tag{14}$$

From (14), the homogenized elastic material properties can be defined as

$$E_{ijkm}^H=\frac{1}{|Y|}\int_Y\left(E_{ijkm}-E_{ijpq}\frac{\partial\chi_p^{km}}{\partial y_q}\right)dY.\tag{15}$$

From the term in ε, it is possible to realize that

$$\boldsymbol{u}^{01}(\boldsymbol{x},\boldsymbol{y})=\boldsymbol{u}^{01}(\boldsymbol{y}).\tag{16}$$

To obtain the linearized elastic buckling response, equation (10) is analysed by setting to zero each of the terms in different ε powers.

Starting with the term in ε^{-2}, considering $\boldsymbol{u}^{10}(\boldsymbol{x},\boldsymbol{y})=\boldsymbol{u}^{10}(\boldsymbol{y})$ and taking into account the periodicity of the displacements, the elastic stability problem at the micro-scale level can be obtained:

$$\int_{\#Y}E_{ijkm}\frac{\partial u_i^{10}}{\partial y_j}\frac{\partial v_k^{10}}{\partial y_m}dY+\int_{\#Y}\sigma_{km}^0\frac{\partial u_c^{10}}{\partial y_k}\frac{\partial v_c^{10}}{\partial y_m}dY=0,\tag{17}$$

$$\forall\;\boldsymbol{v}^{10}\in V_{\Omega\times\#Y},$$

where $\sigma_{km}^0=\sigma_{km}^0(\boldsymbol{x},\boldsymbol{y})$ is the initial stress at micro-scale level resulting from the macroscopic strain field prior to bifurcation and is defined as [1]

$$\sigma_{ij}^0=\left(E_{ijkm}-E_{ijpq}\frac{\partial\chi_p^{km}}{\partial y_q}\right)\frac{\partial u_i^{00}}{\partial x_j}.\tag{18}$$

Equating the term in ε^{-1}, a new expression of the connection between the macroscopic and microscopic instabilities is obtained:

$$\int_{\Omega^{\varepsilon}}E_{ijkm}\left(\frac{\partial u_i^{10}}{\partial y_j}\frac{\partial v_k^{10}}{\partial x_m}\right)d\Omega+\int_{\Omega^{\varepsilon}}\sigma_{km}^0\left(\frac{\partial u_c^{10}}{\partial y_m}\frac{\partial v_c^{10}}{\partial x_k}\right)d\Omega+$$

$$+\int_{\Omega^{\varepsilon}}E_{ijkm}\left(\frac{\partial u_i^{10}}{\partial x_j}\frac{\partial v_k^{10}}{\partial y_m}\right)d\Omega+$$

$$+\int_{\Omega^{\varepsilon}}\sigma_{km}^0\left(\frac{\partial u_c^{10}}{\partial x_k}\frac{\partial v_c^{10}}{\partial y_m}\right)d\Omega=0\forall\;\boldsymbol{v}^{10}\in V_{\Omega\times Y}.\tag{19}$$

As for the term in ε^0, assuming $\boldsymbol{u}^{01}=\boldsymbol{u}^{01}(\boldsymbol{y})$, $\boldsymbol{u}^{10}=\boldsymbol{u}^{10}(\boldsymbol{x})$ and that terms involving the product of three displacement derivatives may be neglected, the macroscopic instability problem is obtained

$$\int_{\Omega^{\varepsilon}}E_{ijkm}^H\frac{\partial u_i^{10}}{\partial x_j}\frac{\partial v_k^{10}}{\partial x_m}d\Omega+$$

$$+\int_{\Omega^{\varepsilon}}\sigma_{km}^{0H}\frac{\partial u_c^{10}}{\partial x_k}\frac{\partial v_c^{10}}{\partial x_m}d\Omega=0\;\forall\;\boldsymbol{v}^{10}\in V_{\Omega\times Y},\tag{20}$$

where

$$\sigma_{ij}^{0H}=E_{ijkm}^H\frac{\partial u_i^{00}}{\partial x_j}.\tag{21}$$

2.1. Finite element formulation

Using the finite element approximation and since $\boldsymbol{u}^{00}=\lambda\boldsymbol{u}$ and $\boldsymbol{u}^{10}=c^{te}\boldsymbol{\phi}$, the macro-scale static elastic problem becomes

$$\boldsymbol{K_x}\boldsymbol{u}=\boldsymbol{F_x},\tag{22}$$

where $\boldsymbol{K_x}$ is the macro-scale stiffness matrix of the structure with homogenized material properties and $\boldsymbol{F_x}$ is the applied reference load vector at macroscopic level.

Similarly, for the micro-structure elastic-static problem, the characteristic displacements are obtained by solving the km linear systems

$$\boldsymbol{K_y}\boldsymbol{\chi}^{km} = \boldsymbol{F_y}^{km}, \tag{23}$$

with $\boldsymbol{K_y}$ being the stiffness matrix related with the unit cell and $\boldsymbol{F_y}^{km}$ the characteristic loading at micro-scale level.

From the solution of the previous equation, the homogenized constitutive matrix can be obtained as follows [1]

$$\boldsymbol{E}_{ij}^{H} = \frac{1}{|Y|}\sum_{e=1}^{N}\int_{Y_e}\left(\tilde{\boldsymbol{\varepsilon}}^i - \boldsymbol{B}_e\boldsymbol{\chi}_e^i\right)^T\boldsymbol{E}_e\left(\tilde{\boldsymbol{\varepsilon}}^j - \boldsymbol{B}_e\boldsymbol{\chi}_e^j\right)dY, \tag{24}$$

where $\boldsymbol{E}_e$ is the element e constitutive matrix, $\tilde{\varepsilon}_i^j = \delta_{ij}$ are 3 independent macroscopic strain fields and $\boldsymbol{\chi}_e$ are the correspondent 3 characteristic displacement fields. Here, the sum has the meaning of a finite element assembly procedure, where N denotes the total number of elements.

For the stability problem of the micro-structure, the finite element approximation leads to

$$\left(\boldsymbol{K_y} + \lambda_y\boldsymbol{G_y}\right)\boldsymbol{\phi} = 0, \tag{25}$$

where $\boldsymbol{G_y}$ is the geometric stiffness matrix and λ_y the load factor for the unit cell.

In the same way, for the macro-scale case, it is obtained

$$\left(\boldsymbol{K_x} + \lambda_x\boldsymbol{G_x}\right)\boldsymbol{\phi} = 0, \tag{26}$$

where $\boldsymbol{G_x}$ is the geometric stiffness matrix and λ_x the load factor at the macro-scale level.

3. Topology optimization for buckling strength maximization

Here the optimization problem is stated as the one of finding the material distribution that maximizes the structure's buckling strength. Mathematically, considering a constraint on the material volume, the problem can be formulated as follows [4].

$$\begin{aligned}
\text{find}: \quad & \mathbf{x} \\
\text{minimize}: \quad & \frac{1}{\lambda_{cr}} \\
\text{subject to}: \quad & \boldsymbol{g}(\mathbf{x}) = \frac{V(\mathbf{x})}{V_0} - f' \leq 0 \\
& \boldsymbol{K}(\mathbf{x})\boldsymbol{U}(\mathbf{x}) = \boldsymbol{F} \\
& \left(\boldsymbol{K}(\mathbf{x}) + \lambda_{cr}\boldsymbol{G}(\mathbf{x},\boldsymbol{U}(\mathbf{x}))\right)\boldsymbol{\phi} = 0 \\
& \mathbf{x}_{min} \leq \mathbf{x} \leq \mathbf{1}
\end{aligned} \tag{27}$$

where $\mathbf{x}$ is the vector of design variables, V is the material volume, V_0 is the design domain volume and f' is the maximum allowed total volume fraction.

Here, a density-based approach is used, meaning that the design variables are the material densities x_e and the element e Young's modulus is determined by x_e. To avoid the appearance of artificial buckling modes, a method proposed in [9] is used,

$$E_k(x_e) = E_0 + x_e^p(E_1 - E_0), \tag{28}$$

$$E_\sigma(x_e) = x_e^p E_1, \tag{29}$$

where $E_k(x_e)$ and $E_\sigma(x_e)$ are the interpolations used to build $\boldsymbol{K}$ and $\boldsymbol{G}$, respectively, E_0 is the Young's modulus assigned to void regions, E_1 the one of the solid material and p is the penalization factor ($p > 1$ and typically $p = 3$ [10]).

From this, the element stiffness and geometric stiffness matrices are given, respectively, by

$$\boldsymbol{K}_e(x_e) = E_k(x_e)\boldsymbol{K}_{0e}, \tag{30}$$

$$\boldsymbol{G}_e = E_\sigma(x_e)\boldsymbol{G}_{0e}\left[\boldsymbol{u}_e(x_e)\right], \tag{31}$$

where $\boldsymbol{K}_{0e}$ and $\boldsymbol{G}_{0e}$ are, respectively, the stiffness and geometric stiffness matrices for an element with unitary Young's modulus.

The optimization problem can be solved by generating and solving a sequence of subproblems that are explicit convex approximations of (27) [11]. For that, the MMA [12] is here used, which requires information on the first derivatives/sensitivities of both the objective and constraint functions.

To calculate the objective function sensitivity, the Rayleigh quotient is used to approximate the critical buckling load factor [4],

$$\frac{1}{\lambda_{cr}} = \max_{\boldsymbol{\phi}\in\mathbb{R}^n,\boldsymbol{\phi}\neq\mathbf{0}}\frac{\boldsymbol{\phi}^T\boldsymbol{G}(\mathbf{x},\boldsymbol{U}(\mathbf{x})))\boldsymbol{\phi}}{\boldsymbol{\phi}^T\boldsymbol{K}(\mathbf{x})\boldsymbol{\phi}}, \tag{32}$$

where n is the total number of eigenvalues, assumed positive and $\lambda_1 = \lambda_{cr} < \lambda_2 < ... < \lambda_n$.

Then, the sensitivity of the objective function is

$$\frac{\partial}{\partial x_e}\left(\frac{1}{\lambda_{cr}}\right) = \boldsymbol{\phi}_{cr}^T\left(\frac{\partial\boldsymbol{G}}{\partial x_e} - \frac{1}{\lambda_{cr}}\frac{\partial\boldsymbol{K}}{\partial x_e}\right)\boldsymbol{\phi}_{cr} - \boldsymbol{V}_{adj}^T\frac{\partial\boldsymbol{K}}{\partial x_e}\boldsymbol{U}, \tag{33}$$

where the critical buckling mode is orthonormalized as $\boldsymbol{\phi}_{cr}^T\boldsymbol{K}\boldsymbol{\phi}_{cr} = 1$, $\boldsymbol{V}_{adj}$ is the adjoint displacement field, solution of the adjoint system [13]

$$\boldsymbol{K}\boldsymbol{V}_{adj} = \boldsymbol{\phi}_{cr}^T\frac{\partial\boldsymbol{G}}{\partial\boldsymbol{U}}\boldsymbol{\phi}_{cr} \tag{34}$$

and the remaining quantities are given by

,

$$\frac{\partial\boldsymbol{K}}{\partial x_e} = px_e^{p-1}(E_1 - E_0)\boldsymbol{K}_{e0}, \tag{35}$$

$$\frac{\partial\boldsymbol{G}}{\partial x_e} = px_e^{p-1}E_1\boldsymbol{G}_{e0}. \tag{36}$$

The derivative of the volume constraint function $g(\mathbf{x})$ with respect to x_e, is, when all finite elements are equal,

$$\frac{\partial g(\mathbf{x})}{\partial x_e} = \frac{1}{n}, \tag{37}$$

where n denotes the total number of elements.

To overcome numerical instabilities, a density filter [14] [15] is here used,

$$\tilde{x}_e = \frac{1}{\sum_{i \in N_e} H_{ei} v_i} \sum_{i \in N_e} H_{ei} v_i x_i, \tag{38}$$

where $\tilde{x}_e$ are the filtered densities N_e is the set of elements i for which the center-to-center distance $\Delta(e,i)$ to element e is smaller than the filter radius r_{min}, H_{ei} is a weight factor defined by $H_{ei} = max(0, \Delta(e,i))$ and v_i is the volume of element i. The application of this regularization requires the modification of the sensitivities by means of the chain rule [10] and the results should always be shown using the filtered density field [16].

4. Methodology and Implementation

The problems discussed in this work, were all implemented by developing Matlab functions, where four node isoparametric plane elasticity elements and plane stress relations were used.

4.1. Elastic buckling at separated macro- and micro-scale problems

Before implementing the buckling problems, the homogenization method was first addressed. The used numerical model was based in the *homogenize* Matlab function presented in [17]. Using the indications provided in [17], the code was modified to calculate the effective material properties of a solid containing one material and void in plane stress. Furthermore, some code lines that enable the visualization of the unit cell configuration resulting from the characteristic displacements were added.

Then, since for plane elasticity buckling eigenvalue problems the required geometric stiffness matrix is obtained in the same way (considering the same element type and apart from the calculation of the initial stress tensor), the Matlab function *Macro_nm* was developed to calculate the critical load for the simpler case of a structure built from a homogeneous solid (with no micro-structure).

To treat the macroscopic instability problem for solids with periodic micro-structure, a Matlab function, *Macro_ms*, was developed. It uses the *homogenize* function to obtain the effective material properties for the calculation of the initial stress tensor, $\boldsymbol{\sigma}^{\mathbf{0}\boldsymbol{H}} = \boldsymbol{E}_e^H \boldsymbol{e}_e$, used to obtain the geometric stiffness matrix.

To address the micro-scale buckling problem, another Matlab function, *micro-buckles* was built, where the *homogenize* function is used to obtain the characteristic displacements, from which the initial stress tensor, $\boldsymbol{\sigma}^{\mathbf{0}} = \boldsymbol{E}_e(\boldsymbol{I} - \boldsymbol{B}_e\boldsymbol{\chi}_e)\boldsymbol{e}_e$, is computed and used to obtain the geometric stiffness matrix.

4.2. Elastic buckling at coupled-scale problems

To implement the coupled instability problem, equation (19) must first be studied.

Because in equation (19) the integrations are performed in the macroscopic domain, the resultant global matrices can be obtained by the assemblage of macro-elemental ones. Furthermore, a macroscopic element can be seen as a domain discretized by microscopic elements. Following this line of thought, the macro-scale element matrices can be obtained by the assembly of micro-scale element matrices corresponding to the micro-elements within the respective macro-element.

If the same element type and discretization are used at both scales, which is assumed not to make the two domains equal, then the nodes of macro- and micro-elements are the same and the assembly operations within each macro-element drop out.

With a double discretization of the model (one at the macro-scale and another at the micro-scale), the instability modes are interpolated by their nodal values:

$$\phi_1(x_1, y_1) \approx \sum_{I=1}^{NN} \phi_1^I N_x^I + \sum_{i=1}^{nn} \phi_1^i N_y^i, \tag{39}$$

$$\phi_2(x_2, y_2) \approx \sum_{J=1}^{NN} \phi_2^J N_x^J + \sum_{j=1}^{nn} \phi_2^j N_y^j, \tag{40}$$

where NN denotes the number of nodal points per macroscopic element, nn the number of nodes per microscopic element and N the shape functions.

This means that the introduction of the approximations (39) and (40), as suggested by [7], results in the following system of equations

$$(\boldsymbol{K_{xy}} + \lambda_{xy}\boldsymbol{G_{xy}})\,\boldsymbol{\phi} = 0. \tag{41}$$

The coupled stiffness matrix, $\boldsymbol{K_{xy}}$, is obtained by the assembly of the elemental ones given by

$$\boldsymbol{K}_{\boldsymbol{xy}}^{\boldsymbol{E}} = \int_{\Omega^E} \int_{Y^e} \boldsymbol{B}_E^T \boldsymbol{E}_e \boldsymbol{B}_e + \boldsymbol{B}_e^T \boldsymbol{E}_e \boldsymbol{B}_E dY d\Omega \tag{42}$$

and the coupled geometric stiffness matrix,$\boldsymbol{G_{xy}}$, by the assembly of

$$\boldsymbol{G}_{\boldsymbol{xy}}^{\boldsymbol{E}} = \int_{\Omega^E} \int_{Y^e} \boldsymbol{g}_E^T \boldsymbol{\sigma}^{\mathbf{0}}{}_e \boldsymbol{g}_e + \boldsymbol{g}_e^T \boldsymbol{\sigma}^{\mathbf{0}}{}_e \boldsymbol{g}_E dY d\Omega, \tag{43}$$

where e or E refers to a micro- or macro- element, $\boldsymbol{B}$ is the strain-displacement matrix and $\boldsymbol{g}$ is de-

fined as (for a micro-scale element)

$$\boldsymbol{g}_e = \begin{bmatrix} \frac{\partial N_y^1}{\partial y_1} & 0 & \dots & \frac{\partial N_y^{nn}}{\partial y_1} & 0 \\ \frac{\partial N_y^1}{\partial y_2} & 0 & \dots & \frac{\partial N_y^{nn}}{\partial y_2} & 0 \\ 0 & \frac{\partial N_y^1}{\partial y_1} & \dots & 0 & \frac{\partial N_y^{nn}}{\partial y_1} \\ 0 & \frac{\partial N_y^1}{\partial y_2} & \dots & 0 & \frac{\partial N_y^{nn}}{\partial y_2} \end{bmatrix}. \quad (44)$$

Since the discretization of the macro- and micro-domains is equal, $\boldsymbol{g}_E = \boldsymbol{g}_e$ and $\boldsymbol{B}_E = \boldsymbol{B}_e$.

With the previous considerations, a Matlab function, named *Coupleds*, was developed for the calculation of the mixed-scale buckling response.

4.3. Buckling strength maximization problem

To address the topology optimization for maximum buckling strength of structures problem, another function, named *TopOptBuckling*, was made.

Here, the objective function is the inverse of the critical buckling factor (to be minimized) and a constraint on the total volume is imposed.

All the finite element calculations, which include the computation of $\boldsymbol{K}$ and $\boldsymbol{G}$, the solution of the equilibrium equations, and the majority of the quantities required for the calculation of the sensitivities, were performed by means of the developed function *FE_analysis* and then returned to the main function *TopOptBuckling*.

The calculations are performed only for simple eigenvalues (no multiplicity of eigenvalues is considered).

5. Results

5.1. Homogenized material properties

Here, an example from [18] of a square unit cell with a rectangular hole was reproduced using the extended *homogenize* function and plotted against the results there presented. The conditions used in [18] were exactly kept: discretization of the unit cell in 20x20 Q4 isoparametric plane elasticity elements, plane stress relations, where $E_{11} = E_{22} = 30$ and $E_{12} = E_{66} = 10$, unitary length for the unit cell side and hole's dimensions of 0.6 and 0.4 (all quantities used are assumed to have consistent units).

The results for the deformed shapes of the unit cell are presented in figure 1 and a comparison between the results for the components of $\boldsymbol{E^H}$ given by [18] and *homogenize* is shown in table 1.

Table 1: Results comparison from [18] and *homogenize*.

Results	E_{11}^H	E_{12}^H	E_{22}^H	E_{66}^H
From [18]	13.015	3.241	17.552	2.785
From *homogenize*	13.015	3.241	17.552	2.785

5.2. Implementation of a geometric stiffness matrix

The Matlab function *Macro_nm* was used to calculate the critical load of a column to be compared with the analytical solution given by the *Euler's Column Formula*. The column is fixed on the left end and free on the right end, where a compressing load is applied. The analytical solution for this case is $P_{cr} = \frac{\pi^2 EI}{4L^2}$, where L denotes the beam's length, E the Young's modulus of the beam's material and I the moment of inertia of the beam's cross-sectional area.

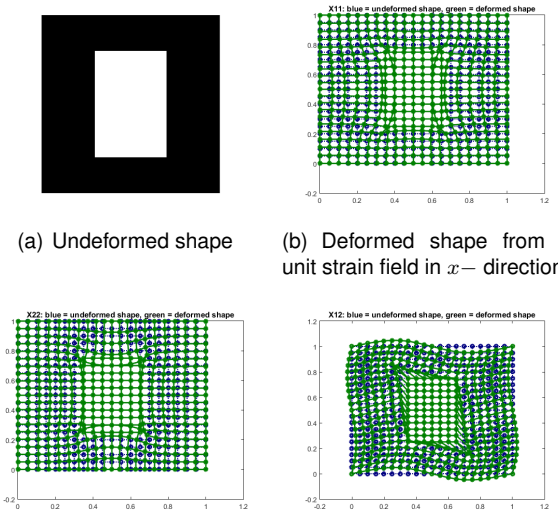

(a) Undeformed shape (b) Deformed shape from a unit strain field in $x-$ direction

(c) Deformed shape from a unit strain field in $y-$ direction (d) Deformed shape from a unit shear strain field

Figure 1: Squared cell with a rectangular hole: undeformed vs. deformed shapes corresponding to the application of three independent unit strains.

The load was applied as a uniform stress distribution of -1MPa in the $x-$ direction. The beam has a length $L = 40$m, a height $h = 5$m and a thickness $b = 1$m. The material has a Young's modulus $E = 2.1$MPa and a Poisson's ratio $\nu = 0.3$.

The body was initially discretized using 16 finite elements and the mesh was progressively refined up to a final value of 800 elements. The convergence tendency of the method with the refinement of the mesh as well as the comparison between the critical loads given by the developed function and the *Euler's Comumn Formula* can be seen in table 2. The two first buckling modes are shown in figure 2.

Table 2: Comparison of the results from *Macro_nm* and the analytical Euler's value (33.734kN).

	Macro_nm					
Nº elements	16	40	120	240	400	800
Pcr [kN]	47.000	42.000	35.500	34.500	34.000	33.500
Error [%]	39.325	24.503	5.235	2.271	0.788	0.694

As it can be seen, the solution converges to the analytical value and the obtained modes agree with the ones known from the literature (see, for instance [19]).

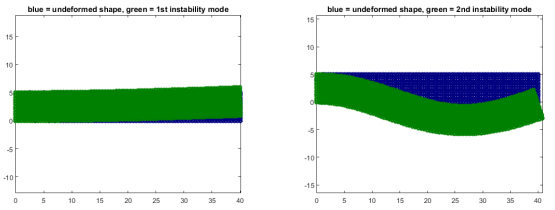

(a) Critical instability mode (b) Second instability mode

Figure 2: First two instability modes: undeformed vs. deformed shapes.

5.3. Micro-scale buckling problem

Here, example 2 from [3] is reproduced using the *micro_buckles* function. In this example, the authors compare the buckling performance of different unit cells with the same material density. The unit cells are discretized using 10x10 Q4 isoparametric plane elasticity elements and are subjected to a macroscopic strain field of $\varepsilon^0 = C^{te}\{-1\ 0\ 0\}$.

The results for the critical load together with the ones presented in [3] are outlined in table 3.

Table 3: Results comparison from [3] and *micro_buckles*.

Case	ρ	λ_{cr} from [3]	λ_{cr} from *microbuckles*
Initial	0.3600	0.1170	0.1177
1	0.5200	0.2080	0.2087
2	0.5200	0.0520	0.0528
3	0.5200	0.0000	0.0000
4	0.5200	0.0000	0.0000

Both the values of the microscopic critical loads and the critical mode shapes were obtained very identically to the ones presented in [3], which enables the validation of the *micro_buckles* function, at least in the presented cases.

5.4. Macro-scale buckling problem

The *Macro_ms* function is applied to a column subjected to a compressing load. Here, the column is built from a solid having a periodic repetition of a squared cell with a squared hole. The base material properties, the column's dimensions and discretization, boundary conditions and loading are the same as in section 4.2.. The unit cell has a material density of 0.64 and an exterior side measuring 0.01m. The homogenized material properties are obtained by discretizing the unit cell in 10x10 Q4 isoparametric finite elements. The results for the critical load are shown in figure 3, where a convergence analysis of the problem is illustrated.

5.5. Mixed-scale buckling problem

Here, two test cases are developed, where the implementation of the mixed-scale buckling problem is applied.

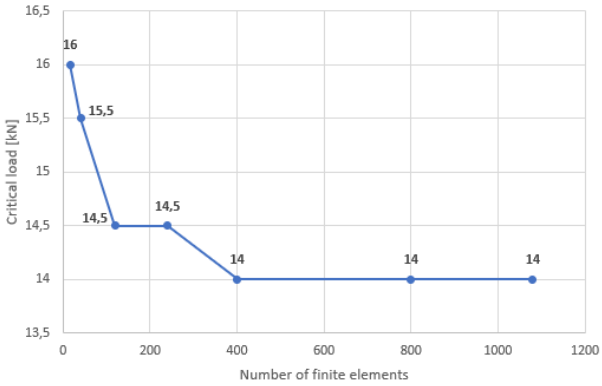

Figure 3: Convergence analysis for *Macro_ms* results of the critical load.

5.5.1 Critical load vs. material density

First, the variation of the critical load with the unit cell's material density for the coupled instability problem is studied and compared with the same variation for the macroscopic buckling case. For that, the previous example of a column (same boundary conditions and loading) is considered. The beam's dimensions are $L = 30$m, $h = 2$m, $b = 1$m; it is built from a periodic repetition of a square unit cell of side 0.5m with a hole and the base material is characterized by $E = 2.1$MPa and $\nu = 0.3$. Starting from a uniform unit cell, the density is decreased by introducing a hole in the microstructure and by progressively increasing its size.

The macroscopic response is obtained by means of the function *Macro_ms* and the double-scale response using the *Coupleds* function. In both cases, the structure is discretized in 24000 finite elements.

The results from both functions are shown if figure 4.

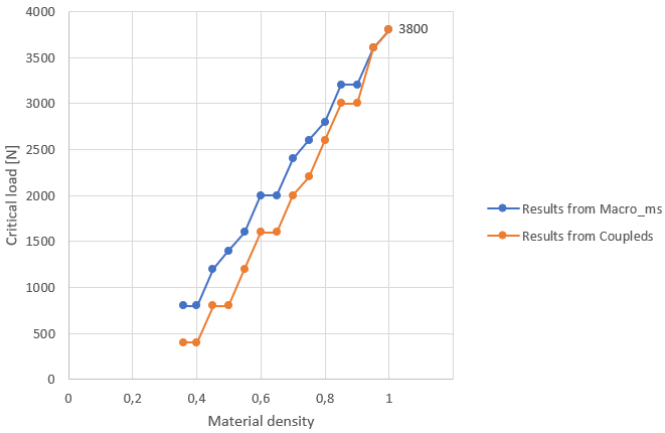

Figure 4: Critical load vs. material density – results from *Coupleds* and *Macro_ms*.

For high values of density it is expected that the results from both functions are equal, since the material is "almost" homogeneous. Particularly, the

case where density equals to one, the result is close to the one given by the *Euler's formula* (error of less than 1%). As density decreases, the *Coupleds* function gives a buckling load lower than that of the *Macro_ms* implementation, since the elastic properties for elements corresponding to void are null in *Coupleds*, whereas in *Marco_ms* these are the homogenized ones.

For all the tested density values, the obtained first and second instability modes were the same as the ones of a macro-scale analysis.

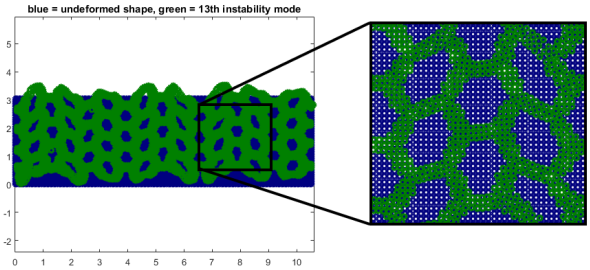

Figure 6: Undeformed shape vs. thirteenth instability mode shape - beam with honeycomb micro-structure.

5.5.2 Column with a honeycomb micro-structure

Here, the objective is to verify if the implementation given by *Coupleds* can capture micro-scale buckling modes.

For that, a beam built from a cellular material with a honeycomb unit cell and subjected to the same boundary conditions and loading as before is considered. The beam's dimensions are L =10.53m, h =3.04m and b =1m, the base material is characterized by $E = 2.1$MPa and ν =0.3, the honeycomb's dimensions are assigned so that its area is unitary [20] and the structure is discretized in 168x48 finite elements.

The micro-scale instability behaviour of the honeycomb is first investigated using the *micro_buckles* Matlab function. Its critical and second buckling modes can be visualized in figure 5. The results showed a critical buckling load factor of 0.0371 ($P_{cr} = 77910$N).

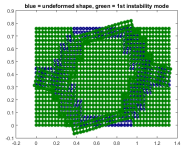

(a) First periodic instability mode for the honeycomb cell

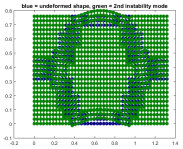

(b) Second periodic instability mode for the honeycomb cell

Figure 5: Honeycomb – micro-scale buckling analysis from *micro_buckles*.

As for the coupled analysis, the first two buckling modes showed none or few buckled unit cells with corresponding buckling loads much lower than the micro-scale critical one. The calculations were then extended to address higher buckling loads. Analysing the thirteenth instability mode shape in figure 6 ($P_{13} = 6382,62$N), one can see a significant number of buckled unit cells. These seem to be arranged in columns and subsequent unstable columns seem to be present in the structure in a mirror-like position, resulting in a deformed but not unstable shape for the remaining cells.

Buckling load values higher than the thirteenth one were considered, where the deformed shape showed no stable cells.

5.6. Buckling strength maximization problem

In this section, a simple example of beam, fixed on the left hand side and subjected to a horizontally distributed compressing load on the right hand side, is optimized for maximum buckling strength using the developed Matlab function *TopOptBuckling*. The beam's dimensions are L=20m, h=5m and b=1m and the applied load has a value of 1Pa. The structure is discretized into 30x8 finite elements and the material parameters are E_1=1Pa, $E_0 = 10^{-6}$Pa and ν=0.3. The structure is optimized for a maximum allowed total volume fraction of 0.6. The penalization factor is p=3 and the filter radius is 0.2m.

The results for the optimized topology and the objective function's history during the optimization iterations are shown in figures 7 and 8, respectively.

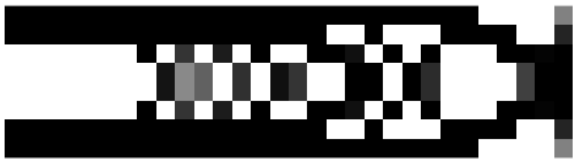

Figure 7: Obtained optimal solution for maximum buckling strength of the beam after 49 iterations.

The objective function converges to a solution throughout the optimization process with only one oscillation. Furthermore, the critical buckling load is raised from 2.66×10^{-3}N up to a final value of 9.63×10^{-3}N, which represents a raise of 266% from the uniform material distribution case.

The final topology presents some areas that can be identified as the so called (and to be avoided) checker-board patterns. However, the solid areas of these regions seem to be aligned with each other, suggesting that these patterns are present due to the poor refinement of the mesh.

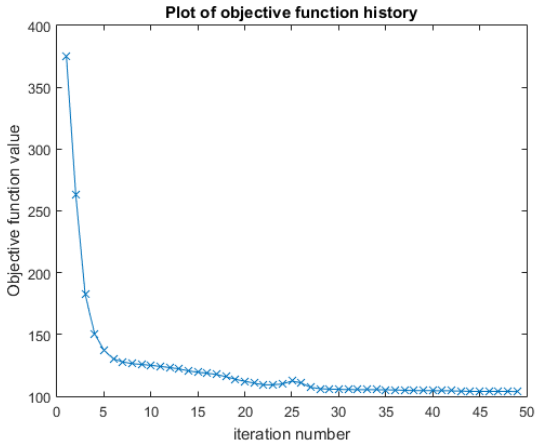

Figure 8: Objective function history for the optimization of the beam.

6. Conclusions

This work provides, numerical implementations to be used in topology optimization of structures and micro-structures for linearized buckling performance maximization as well as the first implementation steps to be carried-out when performing this type of optimization procedure on the macro-scale level.

These are obtained by the application of the finite element approximations to treat the linearized stability problem.

For the case of structures built from cellular periodic materials, the implementations of the stability problems at separated macro- and micro-scales were verified with simple yet illustrative examples from the literature, including the necessary implementation of the homogenization method.

The proposed model of the coupled-scale stability problem enables the application of the mixed-scale instability equation and is capable of capturing macro-scale as well as micro-scale behaviours, at least for the presented examples.

Moreover, the developed implementation for the maximization of the buckling strength of structures converges to a optimal solution.

7. Future work

The given implementation of the coupled-scale instability problem can be further reviewed, namely regarding the validity of using the same discretization for the macro- and micro- domains and the computational efficiency. Furthermore, if this implementation is proven to be valid, since it relies on an equal discretization of the micro- and macro-domains, it could, perhaps, be used in a topology optimization problem to maximize the critical coupled-buckling load of structures. However, since it is developed for structures built from periodic cellular materials, this would possibly require the addition of further constraints on the design variables to ensure the periodicity of the unit cell's topology.

Furthermore, the implementation given for the density based topology optimization for maximized buckling strength yields a basis for including the problem of non-differentiability of the objective function for repeated buckling loads.

Acknowledgments

The author would like to thank Prof. Krister Svanberg for kindly providing his Matlab version of the Method of Moving Asymptotes.

References

[1] C. R. Thomsen, F. Wang, and O. Sigmund. Buckling strength topology optimization of 2d periodic materials based on linearized bifurcation analysis. *Comput. Methods Appl. Mech. Engrg.*, May 2018. https://doi.org/10.1016/j.cma.2018.04.031.

[2] T. W. Chin and G. J. Kennedy. Large-scale compliance minimization and buckling topology optimization of the undeformed common research model wing. In *AIAA SciTechForum*, 2016.

[3] M. M. Neves, O. Sigmund, and M. P. Bendsøe. Topology optimization of periodic microstructures with a penalization of highly localized buckling modes. *International Journal for Numerical Methods in Engineering*, 54:809–834, 2002. DOI: 10.1002/nme.449.

[4] H. C. Rodrigues, J. M. Guedes, and M. P. Bendsøe. Necessary conditions for optimal design of structures with a nonsmooth eigenvalue based criterion. *Structural Optimization*, 9:52–56, 1995.

[5] M. M. Neves, H. Rodrigues, and J. M. Guedes. Generalized topology design of structures with a buckling load criterion. *Structural Optimization*, 10:71–78, 1995.

[6] F. Ferrari and O. Sigmund. Revisiting topology optimization with buckling constraints. *Structural and Multidisciplinary Optimization*, 59:1401–1415, 2019. https://doi.org/10.1007/s00158-019-02253-3.

[7] M. M. Neves. Symbolic computation to derive a linear-elastic buckling theory for solids with periodic microstructure. *International Journal for Computational Methods in Engineering Science and Mechanics*, March 2019. DOI: 10.1080/15502287.2019.1566286.

[8] M. M. Neves. Otimização da topologia de estruturas com constrangimentos de estabilidade. Master's thesis, Instituto Superior Técnico, April 1994.

[9] M. P. Bendsøe and O. Sigmund. *Topology optimization: theory, methods and applications*. Springer, 2nd edition, 2003.

[10] E. Andreassen, A. Clausen, M. Schevenels, B. Lazarov, and O. Sigmund. Efficient topology optimization in matlab using 88 lines of code. In *Structural and Multidisciplinary Optimization*, volume 43, pages 1–16. Springer-Verlag, 2011.

[11] P. W. Christensen and A. Klarbring. *An Introduction to Structural Optimization*. Springer, 2008.

[12] K. Svanberg. The Method of Moving Asymptotes - a new method for structural optimization. *International Journal for Numerical Methods in Engineering*, 24:359–373, 1987.

[13] X. Gao and H. Ma. Topology optimization of continuum structures under buckling constraints. *Comput. Struct.*, 157:142–152, 2015.

[14] T. E. Bruns and D. A. Tortorelli. Topology optimization of non-linear elastic structures and compliant mechanisms. *Comput. Methods Appl. Mech. Engrg.*, 190:3443–3459, 2001.

[15] B. Bourdin. Filters in topology optimization. *Int. J. Numer. Meth. Engrg*, 50:2143–2158, 2001.

[16] O. Sigmund. Morphology-based black and white filters for topology optimization. *Struct. Multidisc. Optim.*, 33:401–424, 2007.

[17] E. Andreassen and C. S. Andreasen. How to determine composite material properties using numerical homogenization. *Computational Materials Science*, 83:488–495, 2014. https://doi.org/10.1016/j.commatsci.2013.09.006.

[18] M. P. Bendsøe and N. Kikuchi. Generating optimal topologies in structural design using a homogenization method. *Computer Methods in Applied Mechanics and Engineering*, 71:197–224, 1988.

[19] S. Timoshenko and J. Gere. *Theory of Elastic Stability*. 2nd edition, 1985.

[20] O. Sigmund. *Design of material structures using topology optimization*. PhD thesis, Technical University of Denmark, 1994.